CHMP3 promotes the progression of hepatocellular carcinoma by inhibiting caspase-1-dependent pyroptosis

YUTING ZHENG[1], SHAOJIE YANG[1], WANLIN DAI[2], JINGNAN WANG[1], SHIYUAN BI[1],
XIAOLIN ZHANG[1], ZHUYUAN ZHENG[1], YANG SUN[1], SHUODONG WU[1] and JING KONG[1]

[1]Department of General Surgery, Shengjing Hospital of China Medical University, Shenyang, Liaoning 110004;
[2]Innovation Institute of China Medical University, Heping, Shenyang, Liaoning 110122, P.R. China

Abstract. Charged multivesicular body protein 3 (CHMP3) is an elemental constituent of the endosomal sorting complex required for transport (ESCRT) III, whose function as a tumor susceptibility gene in the development of liver cancer remains unclear. CHMP3 was found to be associated with pyroptosis by bioinformatics analysis of data from patients with hepatocellular carcinoma (HCC) in The Cancer Genome Atlas database. It was aimed to explore the role and potential mechanisms of CHMP3 in the development of liver cancer. The expression of CHMP3 at the tissue level was examined using immunohistochemistry and western blot analysis. Subsequently, HepG2 and Huh-7 cells were transfected with small interfering RNA and overexpression plasmids to change CHMP3 expression. The proliferative capacity of cells was examined using colony formation and Cell Counting Kit-8 assays. Wound healing and Transwell assays were used to examine the migratory and invasive abilities of the cells. Transmission electron microscopy was used to observe changes in cell morphology. Western blotting was used to examine the expression of caspase-1 signaling pathway related proteins, a classic pathway of pyroptosis. In addition, a xenograft tumor model was used to examine the tumorigenic ability of CHMP3 *in vivo*. The results demonstrated that CHMP3 expression was upregulated in HCC and was associated with poor prognosis. Knockdown or overexpression of CHMP3 inhibited or promoted the proliferation, migration and invasion of liver cancer cells. Knockdown of Huh-7 showed changes in cell membrane integrity as well as cytoplasmic leakage. Furthermore, knockdown of CHMP3 may activate the caspase-1 pyroptosis signaling pathway which in turn inhibits the progression of liver cancer, and this effect can be reversed by the caspase-1 inhibitor AYC. In conclusion, CHMP3 may affect the development of liver cancer through the caspase-1-mediated pyroptosis pathway.

Introduction

Hepatocellular carcinoma (HCC) is the 6th ubiquitous tumor worldwide and the main cause of cancer-related deaths (1). Previous evidence revealed that after decades of dramatic increasing, the incidence of primary liver cancer in men has stabilized, but the incidence in women continues to rise by >2% per year (2). Recently, there have been novel advances in the therapy of precision management of HCC, such as accurate surgical resection, immunotherapy and targeted molecular therapies (3). Patients with multinodular HCC are preferred for hepatectomy and have a satisfactory long-term survival (4). For advanced-stage HCC, the sequence of first-line immunotherapy helps to distinguish relevant clinical and molecular markers for treatment selection (5). Although a large number of newly approved therapies have emerged, the treatment for HCC remains limited and the prognosis is poor (6). Thus, it is considered that the identification of potential therapeutic targets for HCC is an overwhelming and urgent requirement.

Pyroptosis is an inflammatory form of programmed cell death that was first identified in 1992 (7,8). Pyroptosis is caused by caspase-1 activation triggered by inflammasomes, which then cleave interleukin (IL)-1β and IL-18 precursors and mediate the cleavage of gasdermin D (GSDMD) into an N-terminal pore-forming domain, which translocates into the membrane and releases matured IL-1β and IL-18 (9,10). The non-classical pathway does not depend on caspase-1 for activation of the inflammasomes, but rather on lipopolysaccharide-activated caspase-11 or caspase-4/5 (11). Intracellular

LPS-activated caspase-11 directly caused GSDMD cleavage to undergo pyroptosis, whereas caspase-11 activation-induced secretion of IL-1β and IL-18 was indirectly mediated through caspase-1 (12,13). Estrogen suppresses malignant behaviors of HCC cells by targeting the NOD-like receptor thermal protein domain associated protein 3 (NLRP3) inflammasomes (14), suggesting that there is a necessity to understand the mechanisms of pyroptosis-related factors in the proliferation, migration and invasion of HCC.

The Endosomal Sorting Complexes Required for Transport system ((ESCRTs) consists of ESCRT-0, ESCRT-I, ESCRT-II, ESCRT-III and Vps4-VTA1, as well as some accessory proteins (for example ALIX homodimers) which are responsible for catalyzing the sorting of receptors into vesicles on the endosomal membrane to produce multivesicular bodies (15). ESCRT-III complexes, also known as charged multivesicular body proteins (CHMPs), are considered to copolymerize on endosomal membranes (16) and are targets of Vps4, an ATPase associated with various cellular activities that provides energy for ESCRTs to disassemble from the membrane (17,18). CHMP2A and CHMP3 participate in the later stages of ESCRT-III assembly, recruiting VPS4 and preventing Snf7 (CHMP4) aggregation (19,20). A study has found that higher levels of CHMP3 in triple-negative breast cancer (TNBC) predict longer 3- and 5-year outcomes. Overexpression of CHMP3 in TNBC cells suppressed cell growth and invasion through inhibiting EMT process and MAPL (mitochondrial-anchored protein ligase) signaling (21). Moreover, CHMP3 is markedly associated with several biological processes in immunity (for example, cellular response to interleukin-1 or interferon-gamma) and tumor development (for example, primary immunodeficiency) (22). CHMP3 was found to co-occur with mutations in CD8A, and the chromosomal location of the two genes is very similar, which may be cross-synergistic in the process of tumorigenesis (23). There are significant differences in CHMP3 gene expression between multiple myeloma and healthy individuals (24). CHMP3 as a tumor susceptibility gene has been little studied in liver cancer.

In studies related to pyroptosis and HCC, it has been recently reported that CHMP3 may be involved in the pyroptotic process in liver cancer, but no relevant experiments have been conducted to explore this (25). Overall, a growing number of studies have identified a key function of pyroptosis in the development of HCC and in the antitumor process. Therefore, the main aim of the present study was to assess CHMP3 expression in HCC tissues and to demonstrate the effect of CHMP3 on liver cancer cells proliferation, migration and invasion and the possible contribution of pyroptosis.

Materials and methods

Database. RNA sequencing data were derived from the The Cancer Genome Atlas (TCGA) repository for 374 patients with HCC and 50 normal liver samples with corresponding clinicopathological features on 4 August 2021.

Construction of a prognostic model on the basis of differentially expressed genes (DEGs) involved in pyroptosis. A selection of 53 genes associated with pyroptosis were analysed from the available reviews (26,27). The 'limma' data package

is available for screening DEGs. To construct a protein-protein interaction (PPI) network, the Search Tool for the Retrieval of Interacting Genes website (https://string-db.org/) was used. The R (v4.1.3; Robert Gentleman and Ross Ihaka) package 'glmnet' (2.0.16) can be used to narrow down the range of genes to be screened. After central normalization of TCGA dataset ('scale' function in R is applied), risk scores were calculated. The risk score formula is as follows: Risk score=$\sum 8iXixYi$ (X: coefficient, Y: gene expression level). Kaplan-Meier analysis was used to analyze the overall survival (OS) times of patients with hepatocellular carcinoma obtained from the TCGA repository based on the log-rank test with a cut-off value of $P<0.05$. The R package 'prcomp' was used to conduct principal component analysis. Univariate and multivariate Cox regression models were performed to analyze the clinical characteristics of cases in the TCGA cohort.

Survival and expression analysis by Gene Expression Profiling Interactive Analysis (GEPIA) and Human Protein Atlas (HPA). Survival curves of differentially expressed CHMP3 were analyzed by GEPIA (28) to find out whether this gene's expression affects the survival of HCC patients. In addition, the staging plot was analyzed to compare CHMP3 expression in different pathological stages. The expression of CHMP3 was further compared by means of HPA between normal liver and HCC tissues with immunohistochemical (IHC) images.

Clinical materials and sample preparation. Between September 2020 and March 2022, all clinical samples were collected after surgical resection and stored immediately at -80˚C for subsequent experiments at the Department of General Surgery of Shengjing Hospital of China Medical University. All specimens were acquired from patients with HCC confirmed by pathologists. Written informed consent was obtained by all patients whose tissue samples were collected prior to enrolment. Human studies (approval no. 2022PS785K) were approved by the Ethics Committee of Shengjing Hospital of China Medical University (Shenyang, China). Clinicopathological characteristics of patients (including age and sex distribution) are listed in Table I.

IHC staining. The collected tissue was fixed in an appropriate volume of 4% paraformaldehyde at 4˚C for 24 h, then procedurally dehydrated and embedded in paraffin. Tissue sections of 3-μm thickness were produced using a microtome, followed by de-paraffinization using xylene and microwave heating. Sections were placed in the configured antigen repair solution (Citrate antigen retrieval solution; Beyotime Institute of Biotechnology) and boiled for 5 min. Primary antibody against CHMP3 (1:100; cat. no. 15472-1-AP; Proteintech Group, Inc.) was added to the sections after washing with PBS and incubated at 4˚C overnight. The appropriate proportion of HRP-conjugated secondary antibody (ready to use; cat. no. PR30011; Proteintech Group, Inc.) was added, and incubated at 37˚C for 1 h. Antibodies were diluted with TBST, and Tween-20 was used in a dosage of 0.5 ml/l. Finally, chromogenic detection was carried out under the light microscope using DAB. The final score is the percentage of cells multiplied by the staining intensity (29).

Table I. Relationship between CHMP3 expression and the clinical characteristics of 65 patients with hepatocellular carcinoma.

Clinicopathological variables	Total number	Expression level of charged multivesicular body protein 3		P-value
		Low/moderate	High	
All cases	65	21	44	
Age, years				0.952
<55	22	7	15	
≥55	43	14	29	
Sex				0.401
Male	45	16	29	
Female	20	5	15	
Tumor size (cm)				0.013
<5	26	13	13	
≥5	39	8	31	
Preoperative level of alpha-fetoprotein				0.294
<200 μg/ml	25	10	15	
≥200 μg/ml	40	11	29	
Hepatitis B virus				0.915
Negative	22	9	13	
Positive	43	17	26	
Invasiveness				0.766
No	17	5	12	
Yes	48	16	32	

Cell culture. The human liver cancer cell lines HepG2 (Procell Life Science & Technology Co., Ltd.) and Huh-7 (Nanjing KeyGen Biotech Co., Ltd.) cell lines were purchased in August 2021. Cells were expanded and stored at -80°C and only early passages (<passage 5) within 6 months of these cell lines were used in the present study. HepG2 cells were cultured in MEM (Hyclone; Cytiva). Huh-7 cells were cultured in DMEM (Hyclone; Cytiva). Ac-YVAD-CMK (cat. no. GC42721) was purchased form GLPBIO.

Cell line authentication statement. HepG2 and Huh-7 were tested for genotyping of the STR locus and Amelogenin locus using the 20-STR amplification protocol. The results showed that no cross-contamination of human cells was detected in the cell lines and a 100% match to their cytotyping could be found in the cell bank, named HepG2 and Huh-7, respectively.

CHMP3 small interfering (si)RNA and CHMP3 plasmid transfection. Negative control siRNA (siRNA-NC) (UUGTCCGAACGUCUCAAGUTT), small interfering (siRNA)-CHMP3 (UGUGAAGAUUCCAGAGAUUTT), the plasmid vector and plasmid-CHMP3 were purchased from Shanghai GenePharma Co., Ltd. Transfection was carried out at room temperature with Lipofectamine 3000 (GlpBio) following the manufacturer's instructions. Cells were transfected with 2.5 μg RNA/DNA added to 3.75 μl of reagent, and serum-free medium was replaced with complete medium 6 h later. Transfection efficiency was verified by western blotting at 24 h post-transfection. ImageJ (v1.52) (National Institutes of Health) was used to analyze the banding results.

Colony formation. Groups of treated cells were seeded in six-well plates at a density of 1,000 cells/well and cultured in serum-containing medium. The medium was changed every three days and culture was stopped when colony formation was observed with the naked eye. Ac-YVAN-CMK (40 μM, AYC) (GLPBIO) was added to the cells after transfection. Lastly, colonies were fixed with 4% paraformaldehyde for 2 h at room temperature as well as stained with crystal violet solution for 30 min (Beyotime Institute of Biotechnology). More than 50 cells were counted as one colony and then the total number of colonies per well was counted.

Wound healing assay. Groups of treated cells were scratched with a 200-μl pipette tip. The plates were washed with PBS wells to remove residual cells, then serum-free medium was added. Images of the wound shape were captured with a light microscope at a specific point in time (magnification, x200). Wound healing rate=(0 h wound area-48 h wound area)/0 h wound area x100%.

Transwell invasion assay. The Matrigel (Corning, Inc.) was removed from -20°C, placed at 4°C to thaw and melt into liquid form, and then the pre-cooled tip was used to spread the Matrigel evenly on the bottom of upper chamber, followed by placing it in a 37°C incubator for 2-4 h to wait for the Matrigel

to completely solidify. The lower chamber of the Transwell plate was added with 700 μl of serum-containing medium, and the upper chamber was filled with groups of cells resuspended in 200-μl of serum-free medium. The upper chamber was placed in the Transwell plate and incubated for 24 h at 37˚C. Cells from the upper chamber outer membrane were then fixed in 4% paraformaldehyde for 1 h and stained with crystal violet for 30 min at room temperature. Matrigel was wiped from the inner membrane of the upper chamber with a cotton sab and the upper chamber was gently rinsed with PBS to wash away excess color. The invasive cells were observed and images were captured with a light microscope.

Cell Counting Kit-8 (CCK-8) assay. The cell proliferation capacity was assayed according to the manufacturer's instructions of the CCK-8 assay kit (Epizyme; http://www.epizyme.cn/). HepG2 and Huh-7 ($3x10^3$ cells/well) were inoculated into 96-well plates. Cells were transfected with si-CHMP3 and incubated at 37˚C for 24 h before adding AYC (40 μM). A total of 10 μl CCK-8 was then added at each point (24, 48, 72 and 96 h) and incubated at 37˚C for 4 h. The absorbance of the cells at 450 nm was measured using a microplate reader.

Western blotting. Tissue and cell samples were lysed in ice-cold RIPA lysis buffer and PMSF (both from Beyotime, Institute of Biotechnology). The protein concentration was calculated according to the BCA assay kit instructions (Epizyme). Gel electrophoresis separation was performed by 10%- or 15%-PAGE Gel Rapid Preparation Kit (Epizyme) and then transferred to polyvinylidene difluoride membranes (Epizyme). Each lane contained 20 μg of protein. The bands were blocked with 5% skim milk blocking solution prepared in TBST for 2 h at room temperature. After blocking was completed, incubation was carried out overnight at 4˚C using the primary antibodies. The membranes were subsequently incubated for 2 h at room temperature using the HRP-conjugated Affinipure Goat Anti-Mouse/Rabbit secondary antibody (cat. nos. SA00001-1 and SA00001-2, Proteintech Group, Inc.). Protein bands were visualized using an ECL kit (Epizyme). The information of primary antibodies is provided in Table SI.

Transmission electron microscopy (TEM). Huh-7 cells that had been treated differently were collected. The cell pellets were then pre-fixed in 2.5% glutaraldehyde overnight at 4˚C. They were fixed in 1.0% osmic acid for 2 h. The samples were dehydrated and soaked with a 1:1 mixture of epoxy resin and acetone overnight at room temperature. The samples were incubated in 1% uranyl acetate staining solution for 1 h. After 4 days, the samples were sectioned with an ultrathin sectioning machine. Finally, staining was carried out with uranyl acetate and lead citrate. Examination was carried out using TEM.

Xenograft mouse model. In vivo tumor formation was investigated by constructing a xenograft nude mouse model. A total of 18 male BALB/c nude mice (4 weeks old, weighing ~20 g) were used in the animal experiments and were purchased from Beijing HFK Bioscience co. Ltd. All mice were housed under specific pathogen-free conditions (temperature 22˚C; humidity 50%; light/dark cycle 12/12 h), with free access to food and water, and padding changed twice every three days. Huh-7 cells at a density of $1x10^6$ were resuspended in 100 μl PBS to form a cell suspension. Each mouse received a gentle, slow subcutaneous inoculation of 100 μl of cell suspension in the right axilla. When the tumors grew to an optimal volume, the tumor-bearing mice were randomly divided into three groups. siRNA-CHMP3 *in vivo* (10 μg/μl) was incubated with Lipofectamine 3000 for 30 min at room temperature to form siRNA-lipofectamine complexes, which were injected intratumorally every 3 days for 4 weeks. AYC (0.1 mg/kg/day) was injected intraperitoneally every 24 h. Tumor volume (mm^3) was calculated using the following formula: Volume=(width)^2 x length/2. Tumor size was measured every three days. Animal experiments (approval no. 2022PS779K) were approved by the Ethics Committee of Shengjing Hospital, China Medical University (Shenyang, China).

Statistical analysis. The experimental values are shown as the mean ± SEM of at least three independent experiments. One-way analysis of variance (ANOVA) followed by Tukey's multiple comparison test was used to analyze the data with GraphPad Prism (version 9.0.0; Dotmatics). The chi-square test was used to statistically analyze the relationship between different clinical characteristics and CHMP3 expression. Differences between groups were considered statistically significant when P<0.05. All experiments were repeated three times.

Results

Identification of DEGs between normal and tumor tissues. The workflow was summarized in a flowchart (Fig. S1). 39 DEGs (all P<0.05) were recognized through comparing 53 pyroptosis-associated genes' expression in TCGA downloadable data from patients with HCC. From these, 33 genes were upregulated in tumor tissues, while the six other genes exhibited low expression (Fig. S2A). PPI network and an association network containing 20 pyroptosis-associated genes are demonstrated in Fig. S2B and C (red: positive association). When the clustering variable k=2, the intra-group relevance is higher and the inter-group relevance is lower (Fig. S2D). The heat map showed little difference in clinical characteristics between the two clusters except for the degree of tumor differentiation (P<0.001) and OS (P<0.05) (Fig. S2E and F).

Establishment of prognostic gene model in TCGA cohort. Univariate Cox regression was used to find 8 genes that met the criteria of P<0.5 and hazard ratios (HRs) >1 for the next analysis (Fig. S3A). A seven-gene signature was constructed on the basis of the optimal λ values derived from least absolute shrinkage and selection operator Cox regression analysis (Fig. S3B and C). Risk scores were calculated and 424 patients with HCC were divided into low and high-risk groups based on median scores (Fig. S3D). As demonstrated in Fig. S3E-G, it could be concluded that patients in the divided high-risk group clearly had higher mortality and shorter survival compared with the low-risk group. The area under the receiver operating characteristic curve varied from 0.7-0.85, indicating that the prediction model was effective (Fig. S3H).
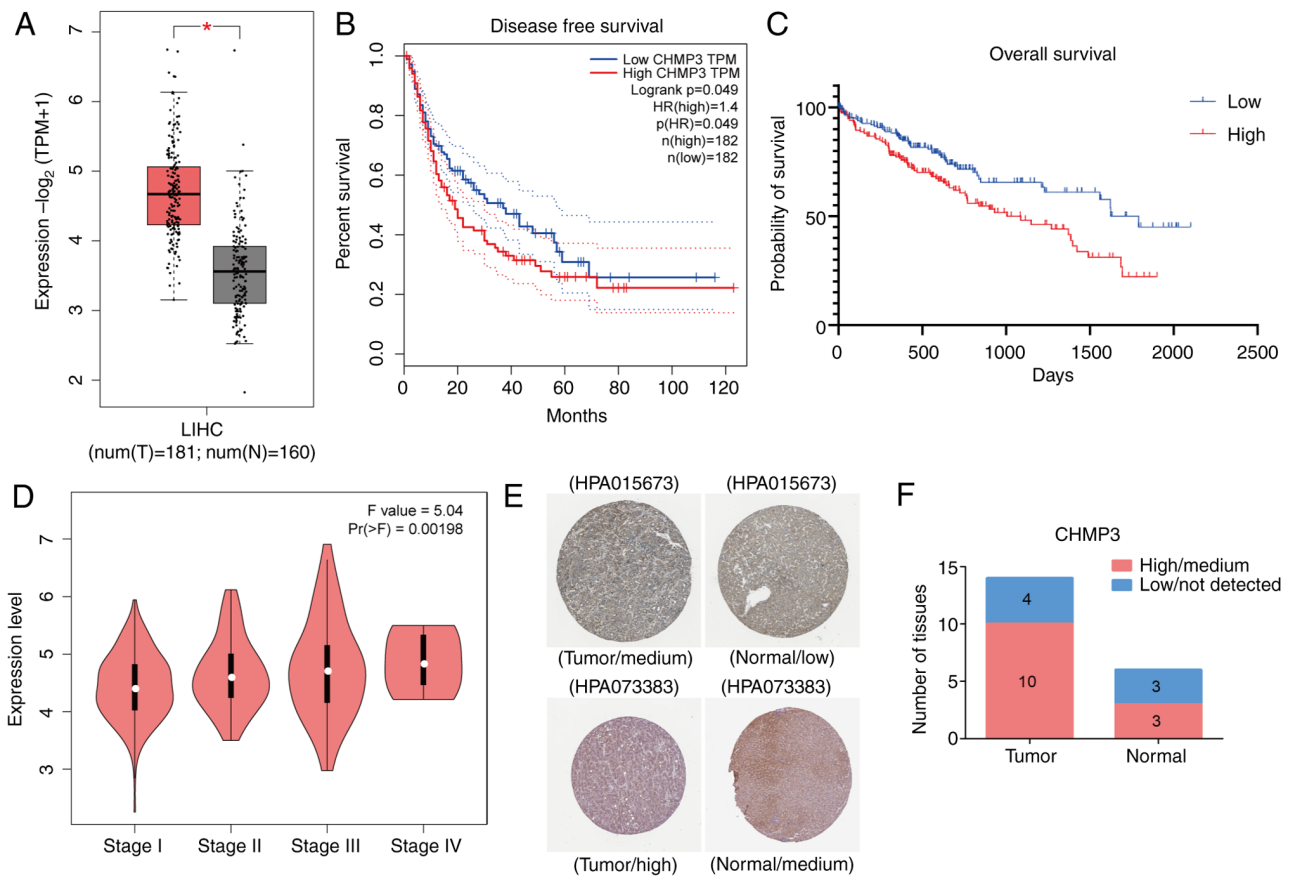
Figure 1. Expression level of CHMP3 in HCC. (A) Verifying the CHMP3 expression in HCC with normal tissues. (B-D) Survival curve (Overall Survival and Disease-Free Survival) and stage plot performed by Gene Expression Profiling Interactive Analysis. (E and F) CHMP3 protein was low detected in normal liver tissues. However, it was highly expressed in liver cancer tissues. CHMP3, charged multivesicular body protein 3; HCC, hepatocellular carcinoma; TPM, transcript per million; LIHC, liver hepatocellular carcinoma.

Independent prognostic value of risk model. Univariate (HR=7.222, 95% Confidence Interval (CI): 4.322-12.066; Fig. S4A) and multifactorial (HR=6.315, 95% CI: 3.638-10.964; Fig. S4B) Cox regression analyses indicated that risk score could be used as an independent predictor of poor survival. Finally, a heat map of clinical features (Fig. S4C) revealed a distinct patient distribution by sex and tumor differentiation in different subgroups (P<0.01). The relationship between CHMP3 and HCC among these seven genes (BAK1, BAX, CHMP3, GSDME, CASP8, GSDMC and SCAF11) remains unstudied. Therefore, the role of CHMP3 in the progression of liver cancer was investigated in the present study.

The relationship between CHMP3 expression and caspase-1 and HCC. As demonstrated in Fig. 1A, CHMP3 was highly expressed in LIHC. The curves of OS and disease-free survival indicated that patients with high expression of CHMP3 presented lower survival rate (Fig. 1B and C). It was also identified that CHMP3 expression varies across pathological stages (Pr (>F) i.e., P<0.05) (Fig. 1D). IHC results obtained from HPA revealed that the expression of CHMP3 was markedly higher in HCC compared with normal tissue (Fig. 1E and F). The database results illustrated two indications: i) CHMP3 participates in the advancement of HCC and, ii) it might be related to pyroptosis.

The CHMP3 expression in HCC tissues. To further validate the results of the public database, the expression of CHMP3 was determined by IHC based on previous predictions. It was found that CHMP3 was apparently overexpressed in the HCC samples compared with the corresponding para-cancer tissues (Fig. 2A-D). The high/low expression is based on tissue type. Another five pairs of carcinoma and para-cancerous tissues were collected to verify the CHMP3 expression and pyroptosis-related proteins by western blot assay, for detecting the level of pyroptosis in HCC. A previous study demonstrated reduced caspase-1 activation and IL-1β expression for some cancers (12). It was then observed that caspase-1, IL-1, IL-18 and GSDMD were significantly downregulated, suggesting the same trend (Fig. 2E and F). Analysis of the clinical characteristics of 65 patients with HCC revealed a significant association between CHMP3 expression and tumor size using the chi-square test (P<0.05).

The CHMP3 expression promotes the proliferation of liver cancer cell lines. According to the aforementioned bioinformatics analysis and the results of IHC and western blotting, CHMP3 was highly expressed in liver cancer. Therefore, CHMP3 was knocked down and overexpressed to observe the effect on the proliferative capacity of liver cancer. The results of western blot analysis showed a significant decrease in CHMP3 expression after transfection with si-CHMP3 in HepG2 and
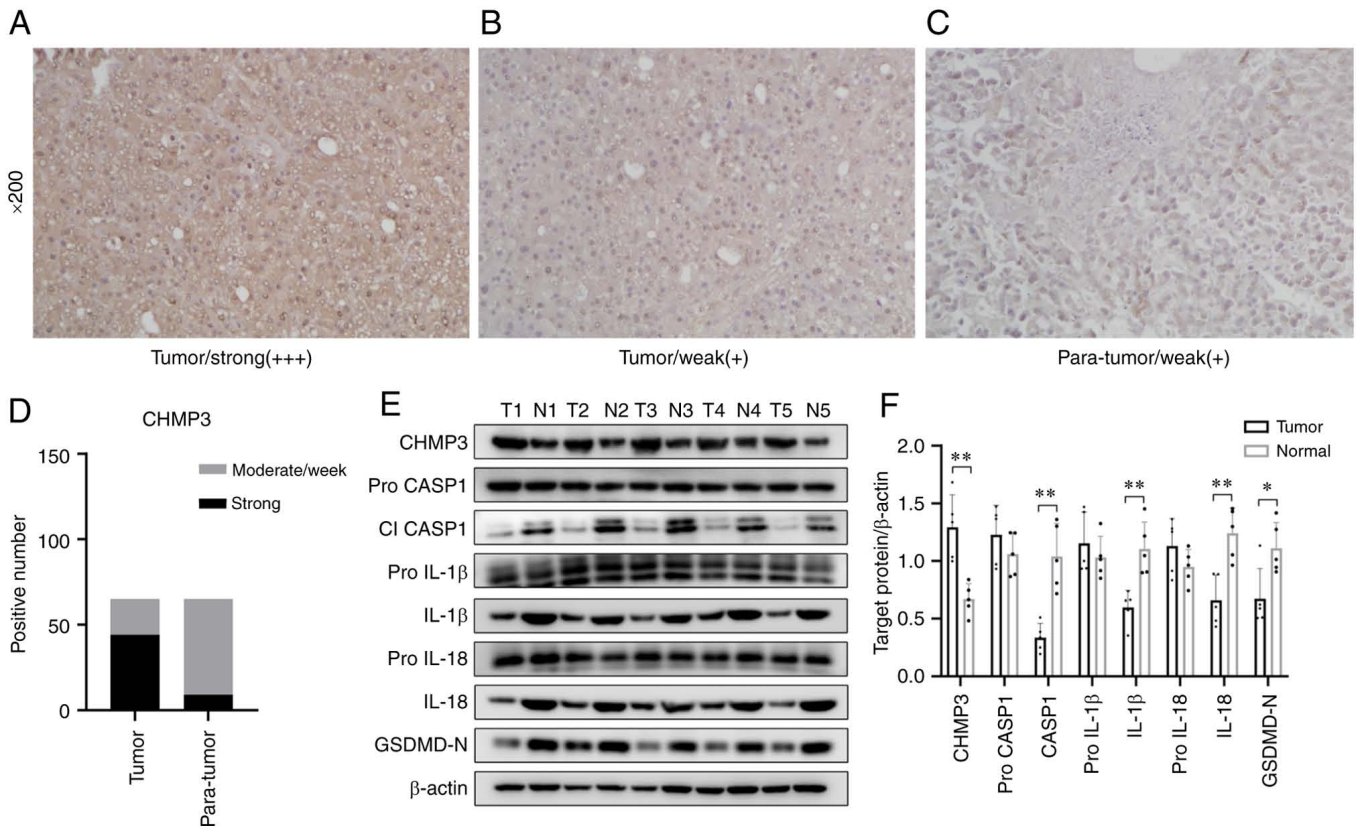
Figure 2. Upregulation of CHMP3 and downregulation of caspase-1 pathway proteins in hepatocellular carcinoma tissues. (A-D) Immunohistochemical staining of CHMP3. (E and F) Western blot analysis of CHMP3 and pyroptosis-related genes expression levels in different tissues. T means tumor tissue and N means normal tissue. *P<0.05 and **P<0.01. CHMP3, charged multivesicular body protein 3; GSDMD, gasdermin D.

Huh-7 cells (Fig. 3A and B). Colony formation assays revealed that knocking down CHMP3 reduced the number of colonies in liver cancer cell lines, which suggests that suppression of CHMP3 impaired the proliferation ability in liver cancer (Fig. 3C-E). On the contrary, cells transfected with plasmid CHMP3 had significantly enhanced colony formation capacity compared with cells transfected with vector (Fig. 3F-J). The transfection efficiency of CHMP3 overexpression was detected by western blotting.

CHMP3 inhibition induces cell membrane blistering and cytoplasm leakage. To explore whether CHMP3 leads to pyroptosis in Huh-7 cells, cellular alterations were observed after knockdown using transmission electron microscopy. It was observed that the transfected cells exhibited typical membrane rupture and cytoplasmic leakage (red arrows) as demonstrated in Fig. 3K. The expression of several proteins was apparently increased after CHMP3 knockdown, including cleaved caspase-1, IL-1β, IL-18 and N-terminal GSDMD (Fig. 3L and M). However, no changes were observed regarding their corresponding precursor forms of expression. Thus, it can be assumed that CHMP3 might promote liver cancer progression through pyroptosis mediated via the caspase-1/IL-1β pathway.

CHMP3 inhibition activates caspase-1 dependent pyroptosis in vitro. To explore whether CHMP3 inhibition-induced pyroptosis is modulated by caspase-1, Ac-YVAD-CMK (AYC, an inhibitor of caspase-1) was used in the present

study. The changes in proliferative capacity of liver cancer was examined after the administration of AYC by colony formation and CCK-8 assays. Knocking down CHMP3 with si-CHMP3 significantly decreased the proliferation of HepG2 and Huh-7 cells, while the application of AYC reversed the ability of si-CHMP3 to reduce cell proliferation (Fig. 4A-F). By carefully examining the data, it was identified that AYC diminished CHMP3 knockdown-induced caspase-1 activation and reduced IL-1β, IL-18 and GSDMD cleavage in liver cancer cells (Fig. 4G and H). Briefly, these data supported the notion that CHMP3 inhibits pyroptosis by caspase-1, and this effect can be reversed by caspase-1 inhibitor.

CHMP3 inhibition activates caspase-1 dependent pyroptosis in vivo. The effect of CHMP3 in tumor formation was then examined *in vivo*. Knockdown of CHMP3 significantly inhibited the growth of subcutaneous tumor, and the volume and weight of the tumor were lower than those of the control group. The addition of AYC reversed this inhibition, indicating that low-expression CHMP3 also inhibited the growth of HCC *in vivo* (Fig. 5A-D).

The relationship between CHMP3 expression and migration and invasion in liver cancer cells. There is a well-known fact that HCC is a highly aggressive and metastatic cancer. In the wound healing assay, the capacity of cell migration was impaired after CHMP3 silencing (Fig. 6A-C) and enhanced after overexpression (Fig. 7A-C). Transwell invasion assay
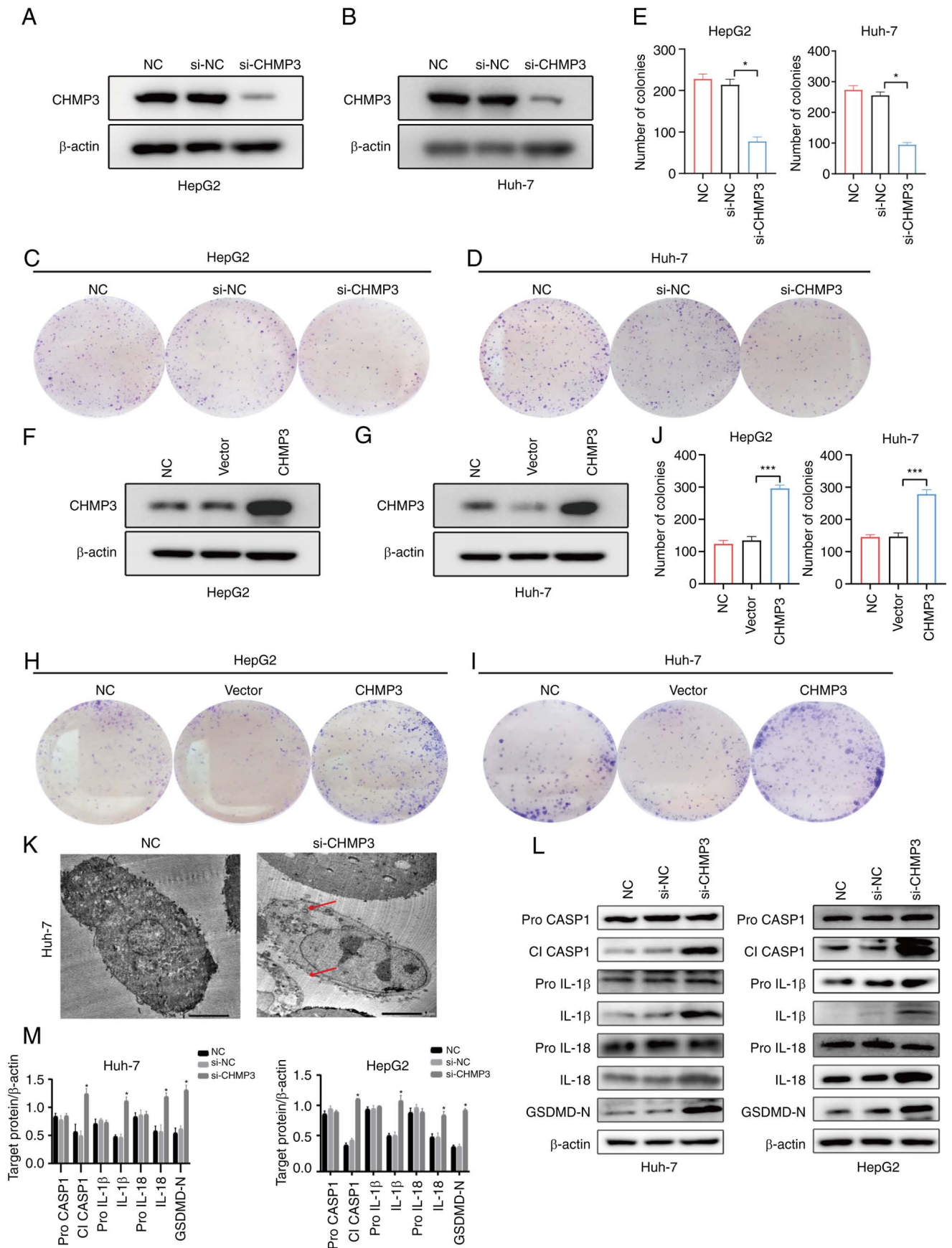
Figure 3. Effect of CHMP3 on the proliferative capacity of liver cancer cells, and its relationship with pyroptosis. (A and B) Western blot analysis of CHMP3 levels following transfection with si-CHMP3. (C-E) Colony formation assays demonstrated the proliferation of HepG2 and Huh-7 cells. (F and G) Overexpressing CHMP3 was evaluated by western blotting. (H-J) The proliferative abilities of the cells overexpressing CHMP3 were higher compared with those of the NC or vector group. (K) Transmission electron microscopy images of cell morphological alterations. (L and M) Western blot analysis of pro caspase-1, cleaved caspase-1, pro IL-1β, IL-1β, pro IL-18, IL-18 and cleaved N-terminal GSDMD levels. $^*P<0.05$ and $^{***}P<0.001$. CHMP3, charged multivesicular body protein 3; GSDMD, gasdermin; si-, small interfering; NC, negative control.
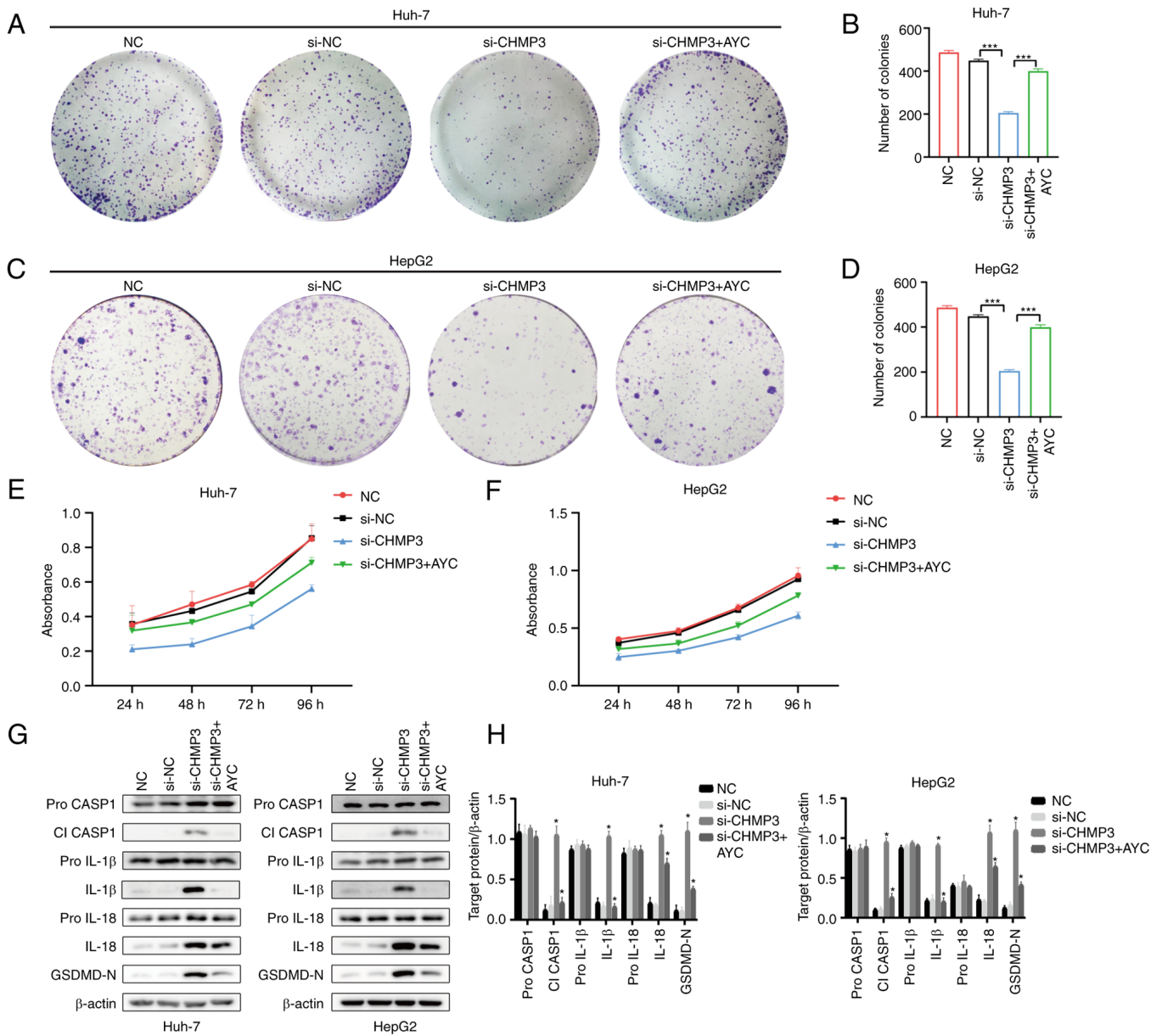
Figure 4. Inhibition of CHMP3 suppresses liver cancer tumorigenesis *in vivo* and *in vitro*. (A-D) Colony formation assay and (E and F) Cell Counting Kit-8 assay demonstrated a reduction in cell proliferation after knockdown of CHMP3, but partial restoration of proliferation capacity after application of AYC. (G and H) Western blotting on changes in protein expression levels after administration of AYC. *P<0.05 and ***P<0.001. CHMP3, charged multivesicular body protein 3; GSDMD, gasdermin; si-, small interfering; NC, negative control.
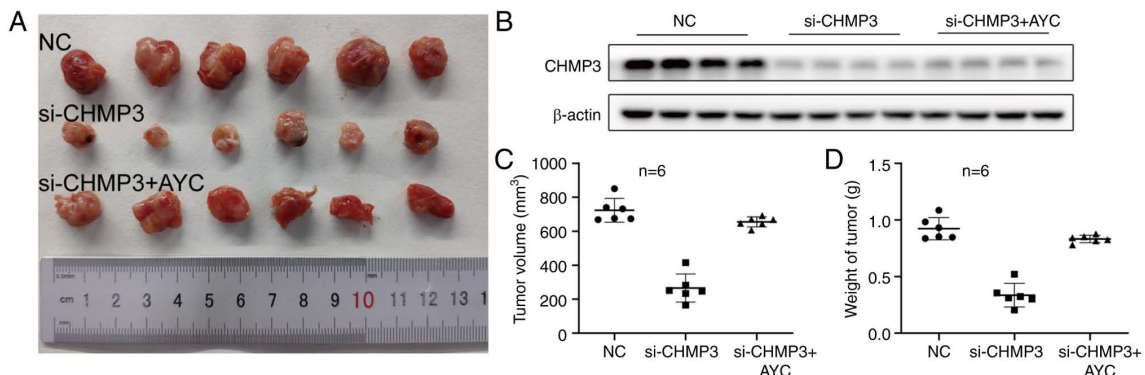
Figure 5. Knockdown of CHMP3 inhibits tumor formation *in vivo*. (A and B) Mouse xenograft assay. Knockdown of CHMP3 reduces tumorigenicity of hepatocellular carcinoma cells according to mouse xenograft experiments. (C and D) Tumor size and weight. After knockdown of CHMP3, the tumorigenic capacity of Huh-7 cells was reduced in both size and weight, and this effect was reversed with AYC (n=6). CHMP3, charged multivesicular body protein 3; si-, small interfering; NC, negative control.
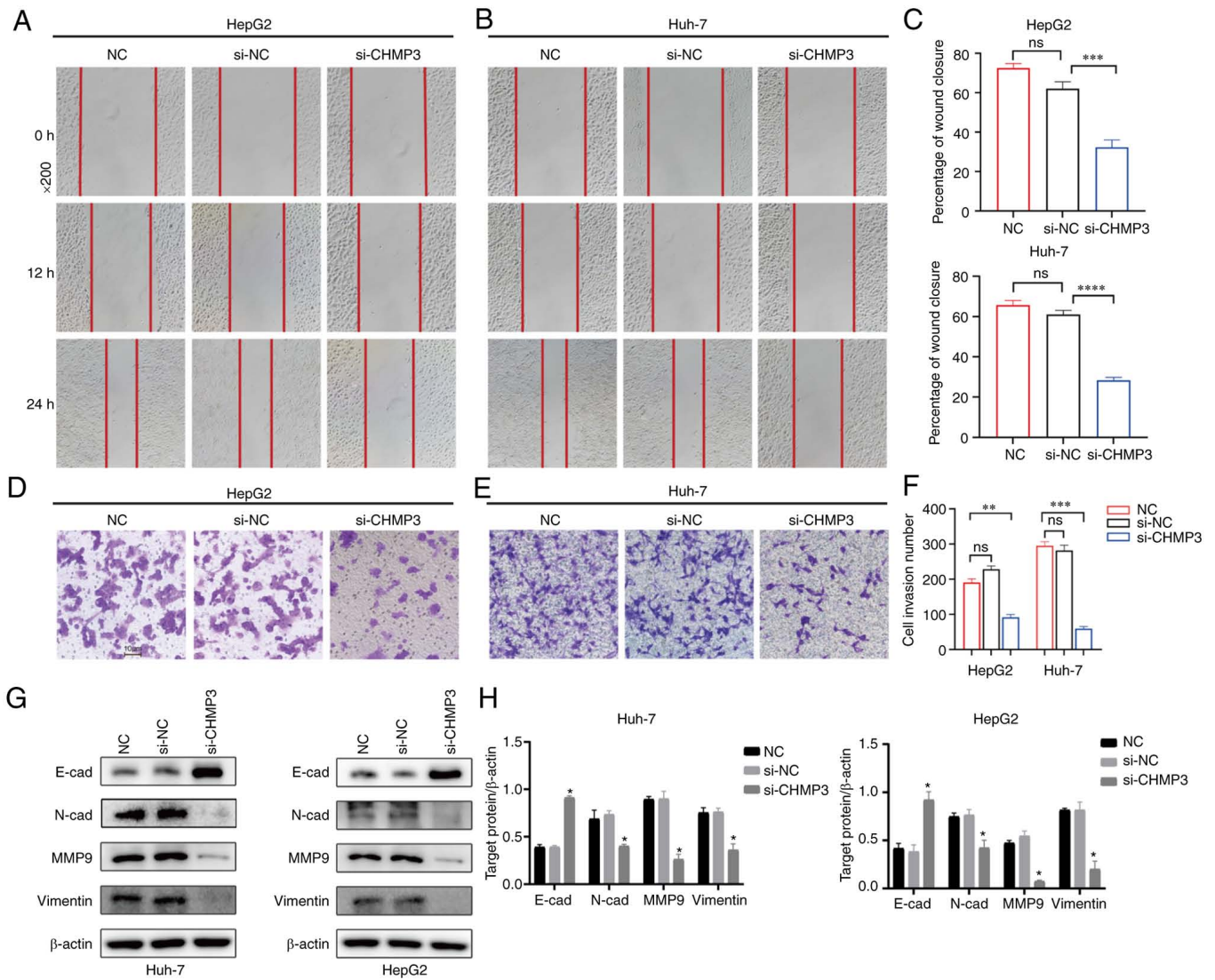
Figure 6. Impact of low CHMP3 expression on the migration and invasion of liver cancer cells and the expression levels of related proteins. (A-C) The wound healing assay results revealed a reduced migratory capacity of si-CHMP3 transfected cells. (D-F) Transwell invasion assay. The number of cells crossing Matrigel was reduced in the knockdown group. (G and H) Western blot examination of changes in the expression of migration-invasion related markers in liver cancer cells transfected with si-CHMP3. $^{*}P<0.05$, $^{**}P<0.01$, $^{***}P<0.001$ and $^{****}P<0.0001$. CHMP3, charged multivesicular body protein 3; si-, small interfering; NC, negative control.

revealed that si-CHMP3 reduced the number of invasive cells (Fig. 6D-F), while CHMP3 overexpression in the plasmid-CHMP3 group increased the number of HepG2 and Huh-7 cells crossing Matrigel (Fig. 7D-F). To provide further evidence of changes in invasion and migration capacity, expression of EMT-related proteins was next investigated in both cells by western blotting. Knocking down CHMP3 caused an significant decrease of N-cadherin, matrix metalloproteinase 9 (MMP9) and vimentin expression, and an increase of E-cadherin expression in liver cancer cells (Fig. 6G and H).

Discussion

Emerging evidence suggests that the impacts of pyroptosis appear to play a different role in liver diseases (11,30). In HCC, a significant reduction in NLRP3 expression suggested a reduced level of pyroptosis (31). NEK7 was found to enhance pathological proliferation of HCC cells *in vivo* and *in vitro*,

while its downregulation inhibited cancer-stromal interactions by causing cancer cell pyroptosis (32).

In the beginning of the present study, the mRNA levels of 53 genes associated with pyroptosis were examined and found to be differentially expressed in both HCC and normal tissues. CHMP3 was then selected as a target for study from the seven gene signatures that had been established. The remaining six genes have been studied with respect to pyroptosis (33-36). However, relatively little research has been conducted on CHMP3 in cancer and cell death. Therefore, exploring the relationship between CHMP3 and the clinical features of HCC can provide an improved understanding of whether CHMP3 can influence the progression of HCC. As expected, patients with higher CHMP3 level showed higher tumor grade and poorer survival conditions. The role of CHMP3 in promoting liver cancer tumor growth at the cellular level was also demonstrated, and its inhibition induced cancer cells to undergo pyroptosis thereby inhibiting liver cancer progression.
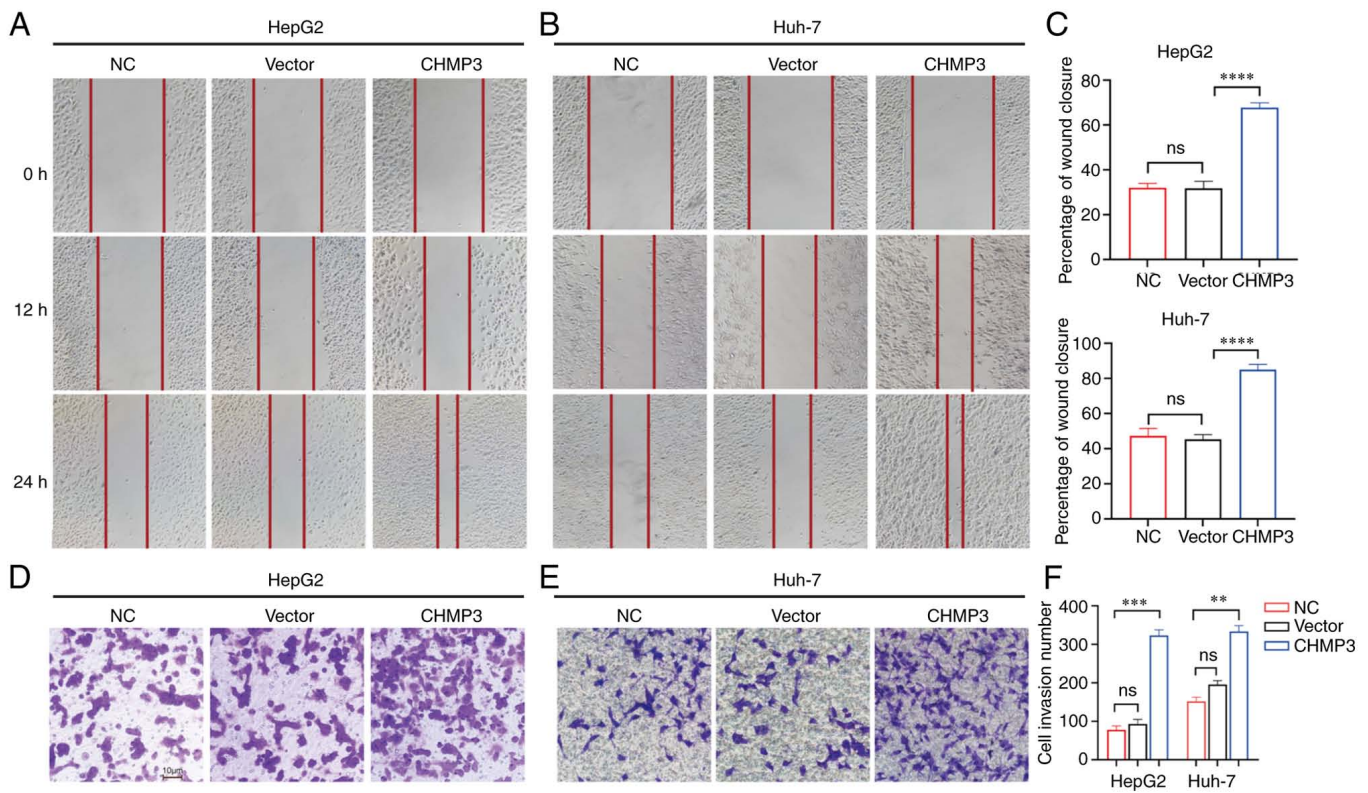
Figure 7. Effect of high CHMP3 expression on the migration and invasion of liver cancer cells. (A-C) Wound healing assay. Faster migration of cells in the overexpression group compared with the NC group. (D-F) Transwell assay. Cells in the overexpression group were more invasive compared with the NC group. [**]P<0.01, [***]P<0.001 and [****]P<0.0001. CHMP3, charged multivesicular body protein 3; NC, negative control.

Over the past decade, pyroptosis and pyroptosis-activated inflammatory factors in human cancers have been increasingly investigated (37-39). The caspase-1/IL-1β pathway affects cell proliferation and other behaviors, and their activation and cleavage enhance cellular pyroptosis and attenuates other pro-oncogenic events (40,41). There is a critical role for this pathway in malignancy invasion, angiogenesis and tumor-immune system interactions (42-44). However, the role of IL-1β in HCC remains controversial, meaning that its expression may either promote or inhibit tumor development. He *et al* (45) and Dang *et al* (46) reported that blocking IL-1β signaling potentially suppressed HCC invasion and metastasis and improved the tumor microenvironment. Nevertheless, a study by Hage *et al* (47) found that dual blockade of IL-1β and IL-18 completely eliminated the anti-HCC effects of sorafenib. Metformin suppressed the development of HCC by cleaving IL-1β and IL-18 through activation of the pyroptosis signaling molecule caspase-1 (48). In addition, it has been demonstrated that CHMP3 knockdown significantly enhanced cellular pyroptosis and IL-1 release (49). In the present study, it was found that the pathway was aberrantly inhibited and that its inhibition may be an oncogenic signaling pathway in liver cancer. When knocking down CHMP3, the caspase-1 precursor did not change, yet its cleaved form increased. Meanwhile electron microscopy revealed changes in the liver cancer cells experiencing pyroptosis. It was hypothesized that knockdown of CHMP3 may be related to caspase-1 activation. Cleavage of GSDMD disrupted the integrity of the cell membrane, which caused the occurrence of cellular pyroptosis.

The mechanisms involved in the present study are illustrated in Fig. 8. Therefore, CHMP3 may control the inflammasome activation and inflammatory factor release.

The pyroptosis is able to inhibit tumor migration and invasion to some extent (40,50). It was found that liver cancer cells with different expression levels of CHMP3 also differed in their ability to migrate and invade. Highly aggressive and metastatic are the most important causes of death for HCC (51). The expression of epithelial calreticulin E-cadherin was reduced, while the expression of N-cadherin, MMP9 and Vimentin was increased when tumor cells metastasized (52-54). N-cadherin is able to increase MMP9 expression which then degrades the extracellular matrix, the vascular basement membrane and the N-cadherin-catenin complex, thereby enabling the promotion of aggressive metastasis of tumor cells (55,56). It was identified that CHMP3 is involved in the migration and invasion of liver cancer by regulating the expression of E-cadherin, N-cadherin, MMP9 and vimentin.

Certain limitations should be considered in the interpretation of the present study. The expression levels of pyroptosis-related genes in resected tumor tissues by western blotting were only detected. It is necessary to continue to explore and improve the relevant experiments in future studies. It is worth considering that the increase in the number of liver cancer cells observed after CHMP3 overexpression may be largely attributable to a decrease in cell death. To improve understanding of the mechanisms involved, the expression of genes known to directly regulate
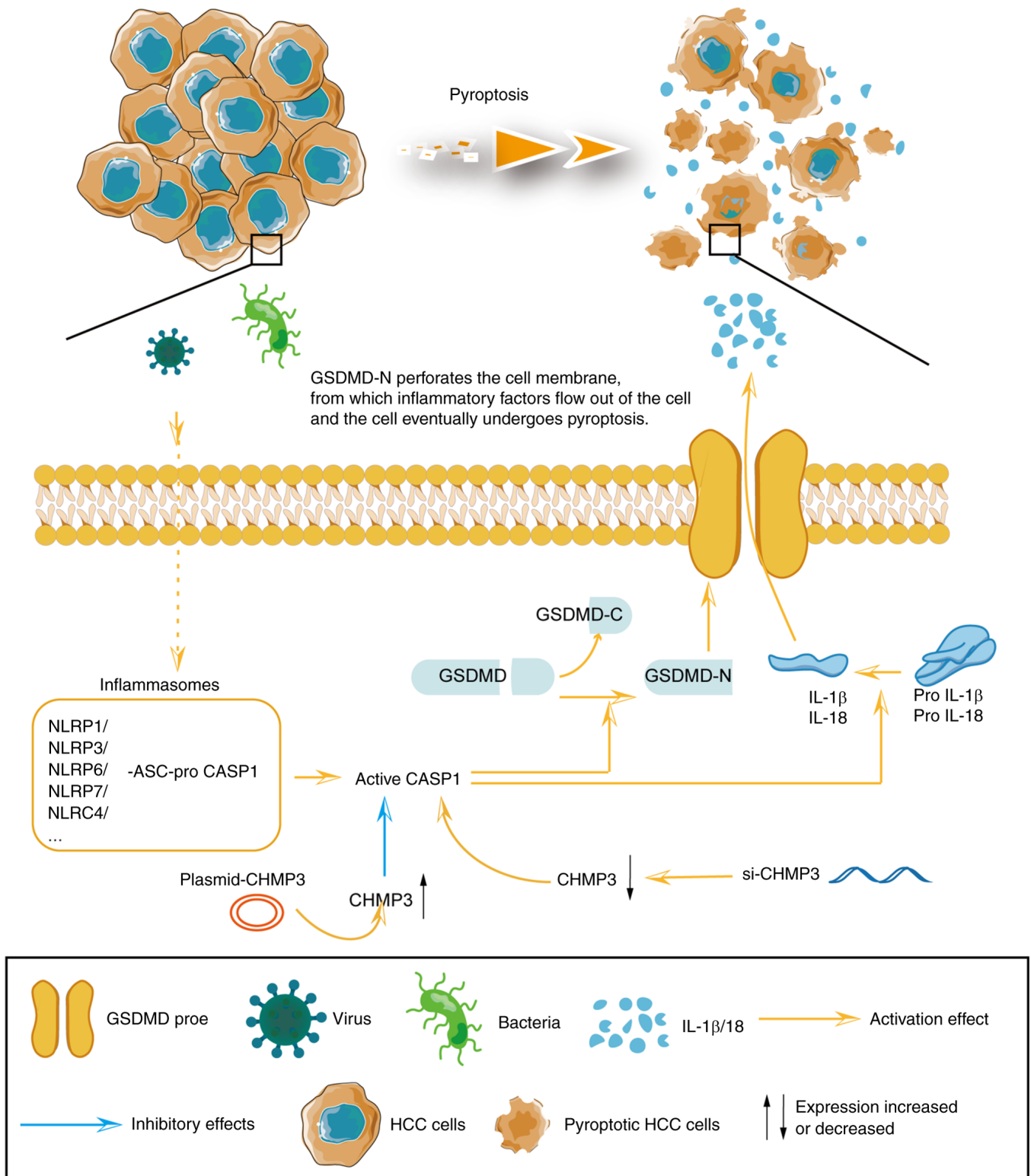
Figure 8. Graphic illustration of CHMP3 regulated the pyroptosis through the caspase-1 signaling axis in HCC. HCC, hepatocellular carcinoma; GSDMD, gasdermin; NLRP3, NOD-like receptor thermal protein domain associated protein 3.

cell proliferation, including CDK, Cyclin D, Rb and E2F, could be investigated in subsequent studies. Evaluating the expression levels of these genes would provide valuable insights into the possible involvement of CHMP3 in the regulation of cell proliferation in liver cancer. Since CHMP3 regulates caspase-1-mediated pyroptosis, which may directly affect tumor immune checkpoint mechanisms, the reduction in tumor size in mice resulting from knockdown of CHMP3 can be attributed, at least in part, to this, rather than to the mere inhibition of cell proliferation.

In conclusion, the function and mechanism of action of CHMP3 in liver cancer was demonstrated. Therefore, CHMP3 may serve as a new prognostic biomarker and therapeutic candidate.

Acknowledgements

Availability of data and materials

The datasets used and/or analyzed during the current study are available from the corresponding author on reasonable request.

Authors' contributions

YZ wrote the manuscript. YZ, SY, WD and JW performed the experiments and generated the figures. SW, SB, XZ, ZZ and YS collected the public and clinic data. JK participated in analyzing and interpreting the data and revised and reviewed the manuscript. All authors made critical revisions, read and approved the final manuscript. All authors confirm the authenticity of all the raw data.

Ethics approval and consent to participate

Written informed consent was obtained by all patients whose tissue samples were collected prior to enrolment. Human studies (approval no. 2022PS785K) and animal experiments (approval no. 2022PS779K) were approved by the Ethics Committee of Shengjing Hospital, China Medical University (Shenyang, China).

Patient consent for publication

Not applicable.

Competing interests

The authors declare that they have no competing interests.

References

1. Chapiro J, Wood LD, Lin M, Duran R, Cornish T, Lesage D, Charu V, Schernthaner R, Wang Z, Tacher V, *et al*: Radiologic-pathologic analysis of contrast-enhanced and diffusion-weighted MR imaging in patients with HCC after TACE: Diagnostic accuracy of 3D quantitative image analysis. Radiology 273: 746-758, 2014.
2. Siegel RL, Miller KD, Fuchs HE and Jemal A: Cancer statistics, 2021. CA Cancer J Clin 71: 7-33, 2021.
3. Tao S, Liang S, Zeng T and Yin D: Epigenetic modification-related mechanisms of hepatocellular carcinoma resistance to immune checkpoint inhibition. Front Immunol 13: 1043667, 2023.
4. Glantzounis GK, Paliouras A, Stylianidi MC, Milionis H, Tzimas P, Roukos D, Pentheroudakis G and Felekouras E: The role of liver resection in the management of intermediate and advanced stage hepatocellular carcinoma. A systematic review. Eur J Surg Oncol 44: 195-208, 2018.
5. Cammarota A, Zanuso V, Manfredi GF, Murphy R, Pinato DJ and Rimassa L: Immunotherapy in hepatocellular carcinoma: How will it reshape treatment sequencing? Ther Adv Med Oncol 15: 17588359221148029, 2023.
6. Ferlay J, Soerjomataram I, Dikshit R, Eser S, Mathers C, Rebelo M, Parkin DM, Forman D and Bray F: Cancer incidence and mortality worldwide: Sources, methods and major patterns in GLOBOCAN 2012. Int J Cancer 136: E359-E386, 2015.
7. Fang Y, Tian S, Pan Y, Li W, Wang Q, Tang Y, Yu T, Wu X, Shi Y, Ma P and Shu Y: Pyroptosis: A new frontier in cancer. Biomed Pharmacother 121: 109595, 2020.
8. Ouyang X, Zhou J, Lin L, Zhang Z, Luo S and Hu D: Pyroptosis, inflammasome, and gasdermins in tumor immunity. Innate Immun 29: 3-13, 2023.
9. Shi J, Zhao Y, Wang K, Shi X, Wang Y, Huang H, Zhuang Y, Cai T, Wang F and Shao F: Cleavage of GSDMD by inflammatory caspases determines pyroptotic cell death. Nature 526: 660-665, 2015.
10. Vande Walle L and Lamkanfi M: Pyroptosis. Curr Biol 26: R568-R572, 2016.
11. Yu P, Zhang X, Liu N, Tang L, Peng C and Chen X: Pyroptosis: Mechanisms and diseases. Signal Transduct Target Ther 6: 128, 2021.
12. Kang R, Zeng L, Zhu S, Xie Y, Liu J, Wen Q, Cao L, Xie M, Ran Q, Kroemer G, *et al*: Lipid peroxidation drives gasdermin D-mediated pyroptosis in lethal polymicrobial sepsis. Cell Host Microbe 24: 97-108.e4, 2018.
13. Pilla DM, Hagar JA, Haldar AK, Mason AK, Degrandi D, Pfeffer K, Ernst RK, Yamamoto M, Miao EA and Coers J: Guanylate binding proteins promote caspase-11-dependent pyroptosis in response to cytoplasmic LPS. Proc Natl Acad Sci USA 111: 6046-6051, 2014.
14. Wei Q, Guo P, Mu K, Zhang Y, Zhao W, Huai W, Qiu Y, Li T, Ma X, Liu Y, *et al*: Estrogen suppresses hepatocellular carcinoma cells through ERβ-mediated upregulation of the NLRP3 inflammasome. Lab Invest 95: 804-816, 2015.
15. Lata S, Schoehn G, Solomons J, Pires R, Göttlinger HG and Weissenhorn W: Structure and function of ESCRT-III. Biochem Soc Trans 37: 156-160, 2009.
16. Babst M, Katzmann DJ, Estepa-Sabal EJ, Meerloo T and Emr SD: Escrt-III: An endosome-associated heterooligomeric protein complex required for mvb sorting. Dev Cell 3: 271-282, 2002.
17. Babst M, Wendland B, Estepa EJ and Emr SD: The Vps4p AAA ATPase regulates membrane association of a Vps protein complex required for normal endosome function. Embo J 17: 2982-2993, 1998.
18. Bishop N and Woodman P: ATPase-defective mammalian VPS4 localizes to aberrant endosomes and impairs cholesterol trafficking. Mol Biol Cell 11: 227-239, 2000.
19. Saksena S, Wahlman J, Teis D, Johnson AE and Emr SD: Functional reconstitution of ESCRT-III assembly and disassembly. Cell 136: 97-109, 2009.
20. Teis D, Saksena S and Emr SD: Ordered assembly of the ESCRT-III complex on endosomes is required to sequester cargo during MVB formation. Dev Cell 15: 578-589, 2008.
21. Wang Z and Wang X: miR-122-5p promotes aggression and epithelial-mesenchymal transition in triple-negative breast cancer by suppressing charged multivesicular body protein 3 through mitogen-activated protein kinase signaling. J Cell Physiol 235: 2825-2835, 2020.
22. Zhou Y, Zheng J, Bai M, Gao Y and Lin N: Effect of pyroptosis-related genes on the prognosis of breast cancer. Front Oncol 12: 948169, 2022.
23. Niu D, Chen Y, Mi H, Mo Z and Pang G: The epiphany derived from T-cell-inflamed profiles: Pan-cancer characterization of CD8A as a biomarker spanning clinical relevance, cancer prognosis, immunosuppressive environment, and treatment responses. Front Genet 13: 974416, 2022.
24. Li C, Liang H, Bian S, Hou X and Ma Y: Construction of a prognosis model of the pyroptosis-related gene in multiple myeloma and screening of core genes. ACS Omega 7: 34608-34620, 2022.
25. Li Y, Li Y, Zhang X, Duan X, Feng H, Yu Z and Gao Y: A novel association of pyroptosis-related gene signature with the prognosis of hepatocellular carcinoma. Front Oncol 12: 986827, 2022.
26. Man SM and Kanneganti TD: Regulation of inflammasome activation. Immunol Rev 265: 6-21, 2015.
27. Kovacs SB and Miao EA: Gasdermins: Effectors of pyroptosis. Trends Cell Biol 27: 673-684, 2017.
28. Tang Z, Li C, Kang B, Gao G, Li C and Zhang Z: GEPIA: A web server for cancer and normal gene expression profiling and interactive analyses. Nucleic Acids Res 45: W98-W102, 2017.
29. Liu L, Li Y, Cao D, Qiu S, Li Y, Jiang C, Bian R, Yang Y, Li L, Li X, *et al*: SIRT3 inhibits gallbladder cancer by induction of AKT-dependent ferroptosis and blockade of epithelial-mesenchymal transition. Cancer Lett 510: 93-104, 2021.

30. Jia C, Chen H, Zhang J, Zhou K, Zhuge Y, Niu C, Qiu J, Rong X, Shi Z, Xiao J, et al: Role of pyroptosis in cardiovascular diseases. Int Immunopharmacol 67: 311-318, 2019.

31. Wei Q, Mu K, Li T, Zhang Y, Yang Z, Jia X, Zhao W, Huai W, Guo P and Han L: Deregulation of the NLRP3 inflammasome in hepatic parenchymal cells during liver cancer progression. Lab Invest 94: 52-62, 2014.

32. Yan Z, Da Q, Li Z, Lin Q, Yi J, Su Y, Yu G, Ren Q, Liu X, Lin Z, et al: Inhibition of NEK7 suppressed hepatocellular carcinoma progression by mediating cancer cell pyroptosis. Front Oncol 12: 812655, 2022.

33. Chen W, Quan Y, Fan S, Wang H, Liang J, Huang L, Chen L, Liu Q, He P and Ye Y: Exosome-transmitted circular RNA hsa_circ_0051443 suppresses hepatocellular carcinoma progression. Cancer Lett 475: 119-128, 2020.

34. Zhang Q, Chen L, Gao M, Wang S, Meng L and Guo L: Molecular docking and in vitro experiments verified that kaempferol induced apoptosis and inhibited human HepG2 cell proliferation by targeting BAX, CDK1, and JUN. Mol Cell Biochem 478: 767-780, 2023.

35. Sun X, Zhong X, Ma W, Feng W, Huang Q, Ma M, Lv M, Hu R, Han Z, Li J and Zhou X: Germacrone induces caspase-3/GSDME activation and enhances ROS production, causing HepG2 pyroptosis. Exp Ther Med 24: 456, 2022.

36. Hou J, Zhao R, Xia W, Chang CW, You Y, Hsu JM, Nie L, Chen Y, Wang YC, Liu C, et al: PD-L1-mediated gasdermin C expression switches apoptosis to pyroptosis in cancer cells and facilitates tumour necrosis. Nat Cell Biol 22: 1264-1275, 2020.

37. Zhang T, Li Y, Zhu R, Song P, Wei Y, Liang T and Xu G: Transcription factor p53 suppresses tumor growth by prompting pyroptosis in non-small-cell lung cancer. Oxid Med Cell Longev 2019: 8746895, 2019.

38. Tan Y, Chen Q, Li X, Zeng Z, Xiong W, Li G, Li X, Yang J, Xiang B and Yi M: Pyroptosis: A new paradigm of cell death for fighting against cancer. J Exp Clin Cancer Res 40: 153, 2021.

39. Hsu SK, Li CY, Lin IL, Syue WJ, Chen YF, Cheng KC, Teng YN, Lin YH, Yen CH and Chiu CC: Inflammation-related pyroptosis, a novel programmed cell death pathway, and its crosstalk with immune therapy in cancer treatment. Theranostics 11: 8813-8835, 2021.

40. Cui J, Zhou Z, Yang H, Jiao F, Li N, Gao Y, Wang L, Chen J and Quan M: MST1 suppresses pancreatic cancer progression via ROS-induced pyroptosis. Mol Cancer Res 17: 1316-1325, 2019.

41. Teng JF, Mei QB, Zhou XG, Tang Y, Xiong R, Qiu WQ, Pan R, Law BY, Wong VK, Yu CL, et al: Polyphyllin VI induces caspase-1-mediated pyroptosis via the induction of ROS/NF-κB/NLRP3/GSDMD signal axis in non-small cell lung cancer. Cancers (Basel) 12: 193, 2020.

42. Rébé C and Ghiringhelli F: Interleukin-1β and cancer. Cancers (Basel) 12: 1791, 2020.

43. Yan W, Chang Y, Liang X, Cardinal JS, Huang H, Thorne SH, Monga SP, Geller DA, Lotze MT and Tsung A: High-mobility group box 1 activates caspase-1 and promotes hepatocellular carcinoma invasiveness and metastases. Hepatology 55: 1863-1875, 2012.

44. Lopez-Pastrana J, Ferrer LM, Li YF, Xiong X, Xi H, Cueto R, Nelson J, Sha X, Li X, Cannella AL, et al: Inhibition of caspase-1 activation in endothelial cells improves angiogenesis: A NOVEL THERAPEUTIC POTENTIAL FOR ISCHEMIA. J Biol Chem 290: 17485-17494, 2015.

45. He Q, Liu M, Huang W, Chen X, Zhang B, Zhang T, Wang Y, Liu D, Xie M, Ji X, et al: IL-1β-induced elevation of solute carrier family 7 member 11 promotes hepatocellular carcinoma metastasis through up-regulating programmed death ligand 1 and colony-stimulating factor 1. Hepatology 74: 3174-3193, 2021.

46. Dang Y, Chen J, Feng W, Qiao C, Han W, Nie Y, Wu K, Fan D and Xia L: Interleukin 1β-mediated HOXC10 overexpression promotes hepatocellular carcinoma metastasis by upregulating PDPK1 and VASP. Theranostics 10: 3833-3848, 2020.

47. Hage C, Hoves S, Strauss L, Bissinger S, Prinz Y, Pöschinger T, Kiessling F and Ries CH: Sorafenib induces pyroptosis in macrophages and triggers natural killer cell-mediated cytotoxicity against hepatocellular carcinoma. Hepatology 70: 1280-1297, 2019.

48. Shen Z, Zhou H, Li A, Wu T, Ji X, Guo L, Zhu X, Zhang D and He X: Metformin inhibits hepatocellular carcinoma development by inducing apoptosis and pyroptosis through regulating FOXO3. Aging (Albany NY) 13: 22120-22133, 2021.

49. Rühl S, Shkarina K, Demarco B, Heilig R, Santos JC and Broz P: ESCRT-dependent membrane repair negatively regulates pyroptosis downstream of GSDMD activation. Science 362: 956-960, 2018.

50. Tang Q, Li W, Zheng X, Ren L, Liu J, Li S, Wang J and Du G: MELK is an oncogenic kinase essential for metastasis, mitotic progression, and programmed death in lung carcinoma. Signal Transduct Target Ther 5: 279, 2020.

51. Bruix J, Gores GJ and Mazzaferro V: Hepatocellular carcinoma: Clinical frontiers and perspectives. Gut 63: 844-855, 2014.

52. Kuphal S and Bosserhoff AK: Influence of the cytoplasmic domain of E-cadherin on endogenous N-cadherin expression in malignant melanoma. Oncogene 25: 248-259, 2006.

53. Mondal S, Adhikari N, Banerjee S, Amin SA and Jha T: Matrix metalloproteinase-9 (MMP-9) and its inhibitors in cancer: A minireview. Eur J Med Chem 194: 112260, 2020.

54. Satelli A and Li S: Vimentin in cancer and its potential as a molecular target for cancer therapy. Cell Mol Life Sci 68: 3033-3046, 2011.

55. Walker A, Frei R and Lawson KR: The cytoplasmic domain of N-cadherin modulates MMP-9 induction in oral squamous carcinoma cells. Int J Oncol 45: 1699-1706, 2014.

56. Cao ZQ, Wang Z and Leng P: Aberrant N-cadherin expression in cancer. Biomed Pharmacother 118: 109320, 2019.